A lung-on-chip infection model reveals protective and permissive roles of alveolar epithelial cells in tuberculosis

Authors: Vivek V. Thacker[1*], Neeraj Dhar[1], Kunal Sharma[1], Riccardo Barrile[2], Katia Karalis[2], John D. McKinney[1*]

Affiliations:

[1]School of Life Sciences, Swiss Federal Institute of Technology Lausanne (EPFL), 1015 Lausanne, Switzerland.

[2]Emulate Inc, Boston, MA 02210 United States

*Correspondence to: vivekvthacker@gmail.com, john.mckinney@epfl.ch

Abstract: *Mycobacterium tuberculosis* (Mtb) is spread via aerosolized droplets and makes 'first contact' with a new host in the alveolar space, an interaction largely inaccessible to experimental observation. We establish a lung-on-chip as an infection model for early tuberculosis, where time-lapse imaging at an air-liquid interface reveals the dynamics of early host-Mtb interactions with a spatiotemporal resolution unattainable in animal models. Pulmonary surfactant mediates a non-growing Mtb population in both alveolar epithelial cells (AECs) and macrophages, although AECs are more permissive to Mtb growth. Defective surfactant production leads to uncontrolled rapid Mtb growth in both cell types which can be partially rescued by formulations containing

surfactant phospholipids. AECs thus have both host-protective and pathogen-permissive roles during first contact, which may explain the full spectrum of human disease and inform new therapeutic interventions.

One Sentence Summary: Live imaging in a lung-on-chip model for early tuberculosis reveals pulmonary surfactant significantly attenuates bacterial growth

Main Text:

Tuberculosis (TB), caused by *Mycobacterium tuberculosis* (Mtb), is characterized by extensive host-pathogen interactions that result in diverse outcomes: although the infectious dose can be as low as one, only 5-10% of individuals exposed to TB develop an active infection (*1*). The infection is also strongly influenced by host physiology: only the smallest aerosol droplets containing 1-2 bacilli can be successfully delivered to the site of infection in the alveolar space (*2*, *3*), whose vast surface area is lined with pulmonary surfactant and is only sparsely populated with alveolar macrophages (*4*). The 'first contact' with a naïve host is therefore by default a single-cell interaction, where heterogeneous outcomes may determine the future course of infection. Potential sources of heterogeneity include cell-to-cell differences in macrophage populations (*5*, *6*), infection of alveolar epithelial cells (*7*), and the action of pulmonary surfactant (*8–10*). These factors have not been characterized completely within the native setting in the lung, primarily because experiments in animal models (*11*) cannot provide information about the dynamics of host-Mtb interactions at this stage with sufficient spatiotemporal resolution (*12*, *13*). The most commonly-used model, *in vitro* infection of macrophages with Mtb

(*14*), does provide excellent spatiotemporal resolution but does not reflect the complexity of the tissue environment *in vivo*.

Bottom-up organ-on-chip systems made of polydimethylsiloxane (PDMS) or biocompatible hydrogels recreate host physiology where tissue-level complexity (*15*, *16*) is incorporated in a modular fashion i.e. the number of cellular components, their identity, and environmental complexity can be tailored to mimic key aspects of the relevant physiology e.g., an air-liquid interface (ALI) in a lung-on-a-chip (LoC) (*15*, *17*). These approaches have emerged as crucial tools for the replacement of animal models in drug development, toxicity testing, and for personalised medicine applications (*18*, *19*). Thus far, a less-explored line of enquiry has been to use them as tools or platforms to study host-pathogen interactions (*20*), where they can occupy the middle ground between simple in vitro experiments and an animal model (*21*).

We therefore establish an LoC model for the early stages of TB infection that in conjunction with live-cell time-lapse microscopy, allows us to dissect the infection dynamics for both AECs and macrophages as independent sites of first contact, and study crosstalk between them mediated by pulmonary surfactant.

Lung-on-a-chip model of tuberculosis

We established a lung-on-chip infection model suitable for time-lapse imaging of early events in tuberculosis (Fig. 1A). Freshly isolated mouse alveolar epithelial cells (AECs) comprise a mix of type I cells (Fig. S1A) and type II cells that produce high surfactant (HS) levels (Fig. S1B). Prolonged *in vitro* passage causes all AECs to adopt an intermediate phenotype with low surfactant (LS) levels (Fig. S1C), smaller and fewer lamellar bodies (Fig. S1D, E), and reduced

expression of type I and type II markers (Fig. S1F). HS and LS AECs maintain these phenotypes on-chip even at the air-liquid interface (Fig. 1E, F). AECs (Fig. 1B) and endothelial cells (Fig. 1C) form confluent monolayers on opposite sides of a porous membrane (Fig. 1D) with an air-liquid interface (ALI) mimicking the alveolar environment. Macrophages added to the epithelial face may remain there (Fig. 1B) or transmigrate across the membrane to the endothelial face (Fig. 1C). Inoculation of the LoC with Mtb (Table S1 for inoculum sizes) leads to infection of both macrophages (white boxes in Fig. 1G, J, zooms in Fig. 1I, L) and AECs (yellow boxes in Fig. 1G,J, zooms in Fig. 1H,K), irrespective of surfactant levels (HS in Fig.1G-I; LS in Fig. 1J-L). The LoC model therefore enables us to study the infection dynamics of these very different cell types simultaneously.

Alveolar epithelial cells are a permissive niche for *M. tuberculosis* replication

We used time-lapse microscopy to study host-Mtb dynamics and quantify the intracellular growth of fluorescent Mtb by measuring total fluorescence intensity (Fig. 2). Between 3 and 5 days post infection under HS (Fig. 2, A-D, Movie S1) or LS (Fig. 2, E-H, Movie S2) conditions, intracellular growth of Mtb is highly variable in both AECs (Fig. 2I, K) and macrophages (Fig. 2J, L). The first-contact host cell usually dies by 5 days post-infection; we therefore restricted our analysis of intracellular bacterial growth rates to 2-4 days post infection. Plots of the logarithm of total bacterial fluorescence intensity over time for individual infected cells representing the spread in growth rates show good agreement with linear fits, indicating exponential bacterial growth in AECs (Fig. 2I, K) and in macrophages (Fig. 2J, L). In a substantial fraction of infected cells, total fluorescence intensity of the intracellular bacteria

increases very slowly (growth rate < 1/168 h^{-1}) or decreases over time. In the absence of a validated live/dead marker, we define these infected cells as a "non-growing fraction" (NGF):

$$Non-growing\ fraction = \frac{no\ of\ microcolonies\ (growth\ rate < \frac{1}{168}\ hr^{-1})}{total\ no\ of\ microcolonies}$$

Comparison of the distributions of bacterial growth rates within individual host cells under HS conditions reveals that intracellular growth is significantly faster in AECs than in macrophages (Fig. 2M, $P = 10^{-6}$). In sharp contrast, under LS conditions, the distributions of bacterial growth rates within individual host cells are not significantly different in AECs compared to macrophages (Fig. 2M, $P = 0.64$). In both cell types, the distributions of intracellular bacterial growth rates under HS (Fig. S2A) or LS (Fig. S2B) conditions are broader than the distributions of bacterial growth rates in axenic cultures. The growth rates of intracellular bacteria show no apparent pattern within the lung-on-a-chip in all surfactant conditions, confirming that the observed cell-to-cell heterogeneity of growth rates is not due to spatial heterogeneity (Fig. S3 A, B). Live-imaging demonstrates that AECs are a more permissive niche than macrophages for intracellular replication of Mtb and suggest that AEC-secreted surfactant may play a protective role in both cell types.

Pulmonary surfactant attenuates M. tuberculosis replication in both AECs and macrophages

To understand the role of pulmonary surfactant, we characterised the growth of bacterial mutants which have been reported to be attenuated in the mouse model. Pulmonary surfactant significantly attenuates growth of WT in both AEC and macrophages in both surfactant

conditions (Fig. 3A-D S4A, B, Table S2). This dynamic is however altered in the ΔRD1-like 5'Tn::*pe35* strain deficient in Type VII ESX-1 secretion (*22*). A functional ESX-1 system has been shown to be required for Mtb to escape into the cytosol (*23*), and its secretion is also upregulated during AEC infection (*24*). The absence of surfactant does not lead to rapid growth in both AECs (Fig. 3E, F) and macrophages (Fig. 3G, H), although AECs are more permissive than macrophages in both HS and LS conditions (Fig. S4C, D). When compared to WT, growth is particularly attenuated in both cell types in LS conditions (Fig. S5B, D). ESX-1 secretion is therefore necessary for rapid growth in the absence of surfactant, which also suggests that surfactant itself, either directly or indirectly, reduces ESX-1 levels on the Mtb capsule. This is in line with a recent study reporting that detergents remove EsxA on the Mtb capsule (*25*). Slower growth in AECs might also explain the delayed dissemination of this strain to the spleen (*22*).

A more subtle mutant is the Δ*pcaA* knockout, which has an altered mycolic acid composition in the capsule (*26*) and is transiently attenuated only during the early stages of infection in the mouse model (*27*). In many aspects this strain behaves similar to WT; growth is significantly attenuated in AECs and macrophages by surfactant (Fig. 3I-L), AECs are more permissive than macrophages under HS conditions, but the differences are not significant in LS conditions (Fig. S4E, F). The Δ*pcaA* strain however is also unable to grow as rapidly as WT in LS conditions in both AECs and macrophages (Fig. S5B, D). Recent studies have reported up-regulation of the PcaA enzyme and other mycolic acid biosynthesis pathways in early infection in alveolar macrophages *in vivo*, but not in *in vitro* macrophage infections (*28*, *29*). Our results indicate that LoC model successfully recapitulates the former but not the latter phenotype, an important

validation of the model. Taken together, these results strongly suggest that pulmonary surfactant limits Mtb growth in both cell types.

LoC model in HS conditions accurately reflects *in vivo* attenuation

The differences between both mutant strains relative to WT are subtle; the 5'Tn::*pe35* strain has a fourfold higher NGF fraction in AECs (Fig. 3F), and the Δ*pcaA* NGF fraction in macrophages is ~20% higher (Fig. 3K). The median values of growth rate are not significantly different (Fig. S5 A, C), however small differences in the shapes of the distribution (reflected in the spread of the 1-99 percentile interval in S5 A, C) are rapidly amplified by exponential growth, and can generate significant differences in total bacterial numbers, the typical metric measured in animal experiments. To illustrate this, we simulated a low-dose animal infection (infectious dose=50 at 1 dpi), assumed each microcolony grew only in macrophages and assigned each microcolony a growth rate randomly chosen from the population distributions. Simulations show bacterial numbers of the WT and Δ*pcaA* strains at 2 days post infection (Fig. 4A), are already significantly different (n=100, p=0.018). Over the first week of infection, the relative attenuation of the Δ*pcaA* strain relative to WT monotonically increases (Fig. 4B). Interestingly, the attenuation (and heterogeneity) predicted by this simple model is in good agreement with experimental data at 7 days post infection (and explain the plateauing of this attenuation); whereas the predicted attenuation under LS conditions is more severe than reported (*27*). A similar trend is evident for the 5'Tn::*pe35* strain, whose attenuation with respect to WT in the mouse model (*22*) is better predicted by the HS dataset than the LS dataset (Fig. S6A, B). An even starker example of attenuation is the Δ*icl1*Δ*icl2* knockout that is severely attenuated in vivo (*30*). Even at 6 days

post infection (Fig. S7A-C) of a LS LoC infected with a high multiplicity of infection, there is little or no growth in both AECs and macrophages; many macrophages contain numerous single Mtb bacteria. This lack of growth also rules out the possibility that Mtb grow only extracellularly in the LoC without infecting host cells. These results show that the LoC infection model meets the benchmarks set by data from *in vivo* experiments, the physiology of which is accurately represented by HS conditions.

Hydrophobic surfactant components interact directly with Mtb

Lastly, we tested if Curosurf^{TM}, a pulmonary surfactant replacement formulation composed of phospholipids (39% w/v dipalmitoylphospatidylcholine (DPPC)) and the hydrophobic proteins SP-B and SP-C, could rescue the phenotype observed in LS LoCs. Treatment with a dilute solution of Curosurf either added to the alveolar face for a short period before infection with WT bacteria ('Chiptreat') or allowed to interact with resuspended Mtb cultures prior to the infection of an untreated LS LoC ('Mtbtreat') attenuated growth and generated an NGF (Fig. 5A, Table S2). Curosurf treatment of a single-cell Mtb suspension did not affect Mtb growth *in vitro* (Fig. S8).

One hypothesis is that the attenuation upon infection is due to the direct interaction of surfactant lipids with the Mtb capsule. Images of clumps of Mtb treated with Curosurf doped with a 10% of fluorescently labelled phospatidylcholine (PC) and subsequently washed reveal that the fluorescently labelled PC both incorporates into the surfactant and through surfactant vesicles, coats the bacteria (representative image in Fig. 5B, maximum intensity projection in S9). Additionally, incubation with surfactant increases the amount of total free lipids including

surface mycolic acids such as trehalose dimycolate (TDM) in the supernatant when compared to supernatant without surfactant treatment (Fig. 5C, D). These transient exchange of lipids between the Mtb capsule and surfactant vesicles could explain why surfactant pre-treatment reduces growth.

Discussion

TB is a global health priority in need of new preventive strategies, host-directed therapeutics, and vaccines. Both smokers and the elderly have altered pulmonary surfactant compositions (*31–33*) and an increased risk of developing active TB. In the mouse model, reduced surfactant catabolism in GM-CSF$^{-/-}$ mice might explain rapid disease progression (*34*), however the direct role of AECs has been difficult to study. This is possible in the LoC infection model that uses primary mouse cells, offers superior physiological mimicry, is long-term time-lapse imaging compatible and can be successfully benchmarked with the mouse model. These advantages over other reported co-culture systems for TB (*35–38*) allow us to perturb to host physiology by substantially reducing pulmonary surfactant levels which typically imposes an intolerable animal burden. It has revealed several new biological insights into the dynamics of the earliest host-Mtb interactions mediated by surfactant. When surfactant is reduced, WT Mtb grows more rapidly than *in vitro* axenic culture; a trait that is shared to a lesser extent by mutants attenuated for known virulence factors. In the presence of surfactant, a significant fraction of bacteria do not grow as judged by fluorescent expression levels. It is likely that a majority of these are indeed sterilized, however we do not have definitive proof of this. Nevertheless, they are not active participants in these early stages of infection. On the contrary, AECs are active participants, not only through the production of pulmonary surfactant already discussed but also as a site of first

contact despite being surrounded by macrophages. It is likely that the current LoC model and method of Mtb inoculation exaggerate the incidence of AEC infection; however, this gives us an opportunity to study both AEC and macrophage infections in co-culture at the ALI. The significant differences in outcome between AECs and macrophages in the presence of surfactant suggest that even were AEC infections to occur far more infrequently *in vivo*, it would probably lead to a more aggressive infection.

The exact mechanisms of surfactant-mediated attenuation remain to be elucidated, but this work demonstrates a direct physical interaction that is a two-way street: Mtb surface lipids are actively removed while surfactant lipids coat the bacterial surface. These interactions are independent of the action of hydrophilic SP-A and SP-D proteins that have previously shown to interact with Mtb surface lipids (*39–41*), and enzymes shown to modify the Mtb capsule (*9*, *10*), none of which are components of Curosurf. These components have been shown to be potent adjuvants for intranasal influenza vaccines (*42*), suggesting the possibility that pulmonary surfactant could be harnessed to generate improved therapeutics and host-directed therapies against the spread of TB.

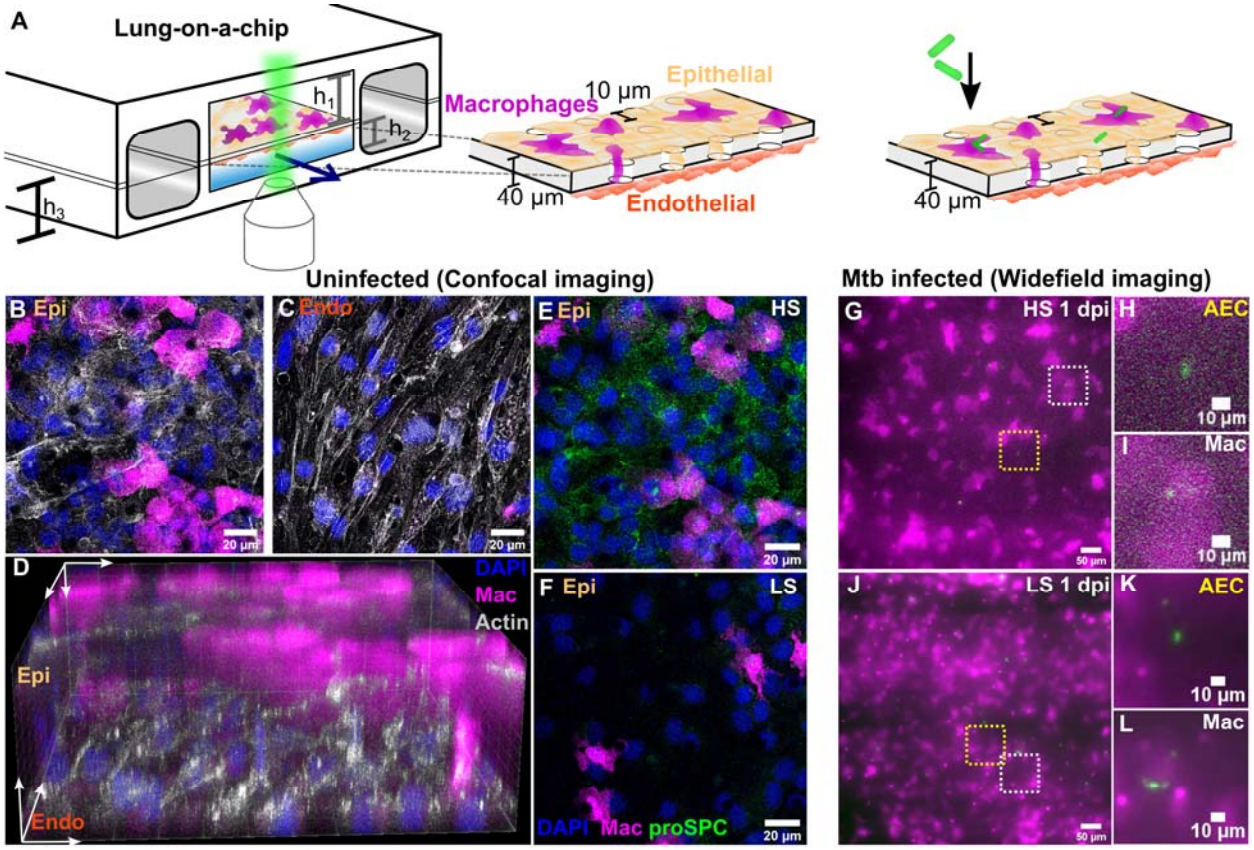

Fig. 1. Lung-on-a-chip (LoC) model of tuberculosis.

(A) Confluent layers of alveolar epithelial cells (AECs) and endothelial cells populate the top and bottom faces of the porous membrane that separates the air-filled "alveolar" (upper) and liquid-filled "vascular" (lower) compartments, creating an air-liquid interface. GFP-expressing macrophages (magenta) are added to the alveolar compartment and may transmigrate to the vascular compartment. Addition of bacteria to the alveolar compartment mimics the natural route of infection. h_1 = 1 mm, h_2 = 250 µm, h_3 = 800 µm. **(B-C)** Confocal microscope images of an uninfected LoC stained to visualize nuclei (blue) and actin (grey); surfactant (green) was stained with an anti-proSPC antibody. Confluency of epithelial **(B)**, and endothelial **(C)** layers is maintained at the air-liquid interface over 7 days, and 3D imaging reveals occupancy of some pores by macrophages **(D)**. LoCs reconstituted with HS **(E)** or LS **(F)** AECs continue to express

high or low levels of surfactant respectively. **(G-L)** Widefield microscope images of LoCs reconstituted with HS **(G-I)** or LS **(J-L)** AECs and infected with a low dose of Mtb expressing td-Tomato (green). Images taken 1-day post-infection show that AECs (yellow boxes **(G, J)** and zooms **(H, K)**) as well as macrophages (white boxes **(G, J)** and zooms **(I, L)**) can be sites of first contact.

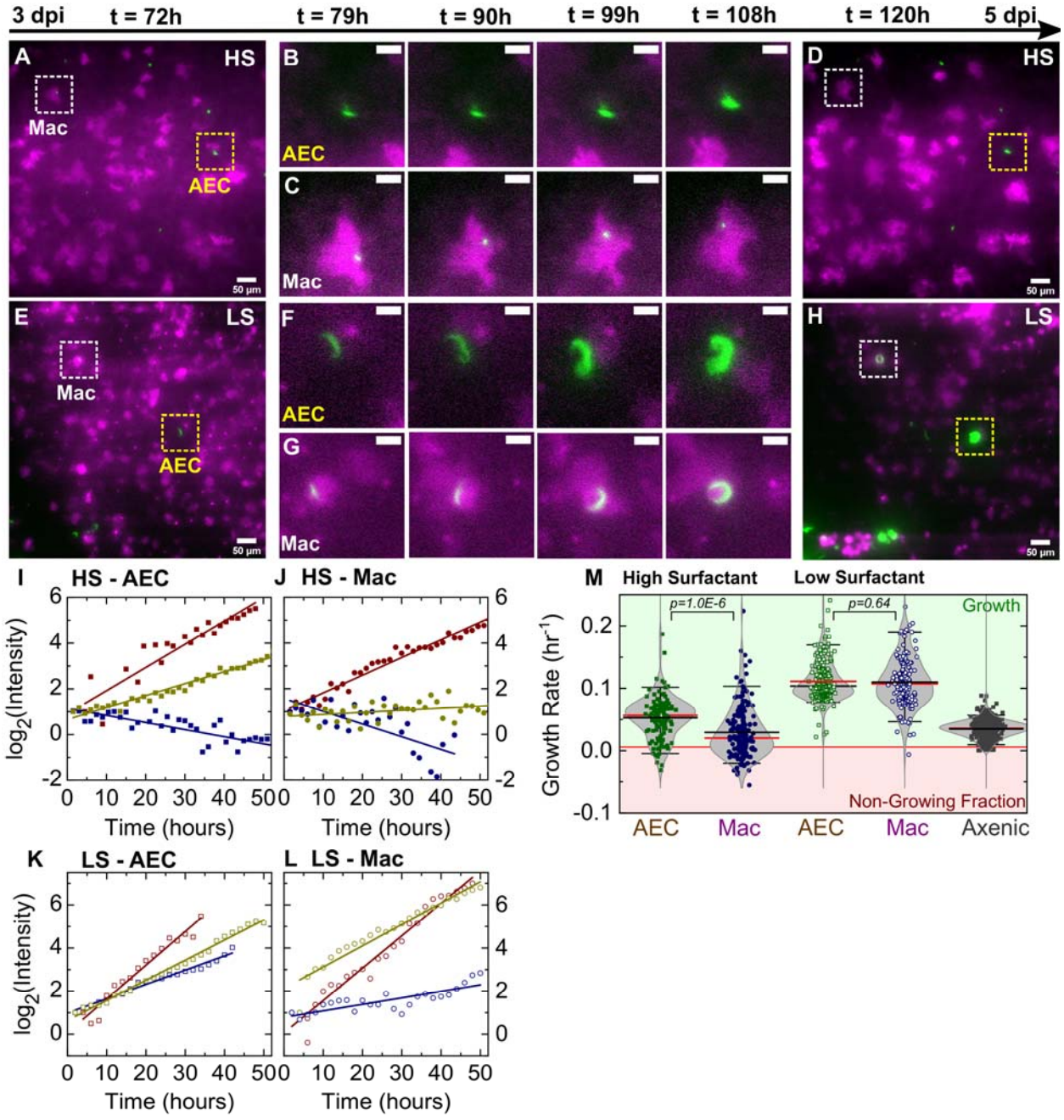

Fig. 2. Live imaging reveals AECs are a permissive niche for Mtb growth. Snapshots from live-cell imaging between 3-5 days post infection (dpi) in both HS **(A-D)** and LS **(E-H)** LoCs. Macrophages are false-colored magenta, Mtb is false-colored green. Representative examples of

AEC (yellow boxes) and macrophage (white boxes) infection are highlighted, zooms **(B, C, F, G)** reveal growth in both cell types over this period. Scale bar = 10 μm. **(I, J)** Plots of the logarithm of total fluorescence intensity vs time confirm exponential growth for representative infections in both AECs **(I, K)** and macrophages **(J, L)** in HS and LS conditions respectively. In each case, a microcolony with growth rate close to the population maximum (red), median (yellow), and minimum (blue) is shown. The growth rate is the gradient of the linear fit. Scatter plots of growth rate for AEC (n=122 for HS, n=219 for LS) and macrophage infections (n=185 for HS, n=122 for LS) reveals growth is significantly faster in AECs than macrophages in HS conditions but not in LS conditions **(M)**, and that there is greater cell-to-cell heterogeneity in both conditions when compared to single-cell Mtb growth rate data from axenic conditions in microfluidic devices. Colonies constituting the non-growing fraction (NGF) fall in the region shaded in red, growth is shaded green. p-values calculated using a Kruskal-Wallis one-way ANOVA test.

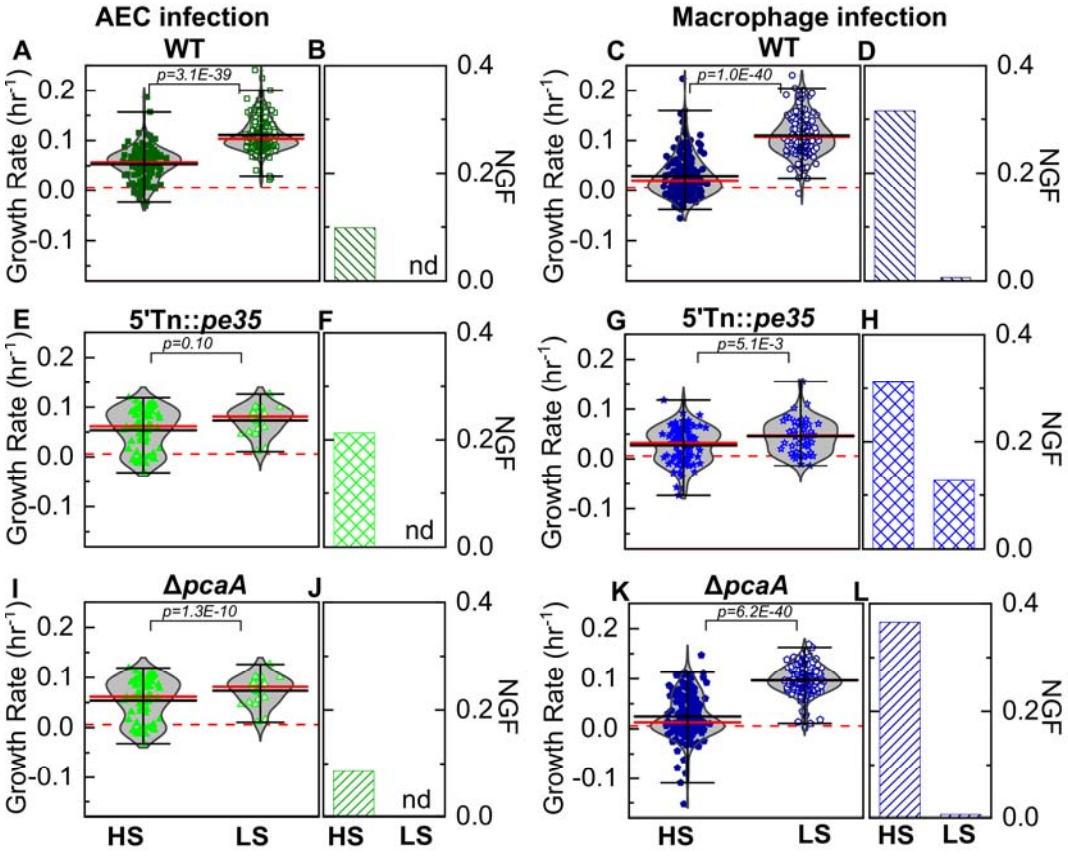

Fig. 3. Pulmonary surfactant plays a host protective role. Scatter plots of growth rate for AEC infection **(A, E, I)** and macrophage infection **(C, G, K),** and bar graphs for non-growing fraction (NGF) for AEC infection (**B, F, J**) and macrophage infection (**D, H, L**) in high surfactant (HS) and low surfactant (LS) conditions for WT, 5'Tn::*pe35*, and Δ*pcaA* strains respectively. 'nd' refers to the absence of NGF. LS conditions significantly increase growth rates and lower NGF in both AECs **(A, B)** (n=122 for HS, n=219 for LS) and macrophages **(C, D)** (n=185 for HS, n=122 for LS) for WT. Differences between HS and LS conditions are not significant for the 5'Tn::*pe35* strain in AECs **(E)** (n=61 for HS, n=25 for LS) and HS conditions generates a high NGF **(F)**. Although differences are statistically significant for macrophages (**G**)

(n=93 for HS, n=55 for LS), there remains a significant NGF in macrophages even in LS conditions **(H)**. In contrast, the Δ*pcaA* strain behaves closer to WT, and reduced surfactant levels also lead to significantly faster growth in both AECs **(I, J)** (n=58 for HS, n=48 for LS) and macrophages (n=172 for both HS and LS) **(K)**, although the NGF fraction in macrophages **(L)** is highest for this mutant. p-values calculated with a Kruskal-Wallis one-way ANOVA test, each dataset is fitted with a non-parametric kernel density estimation characterised by the mean (black) and median (red) values. Whiskers represent the 1-99 percentile interval.

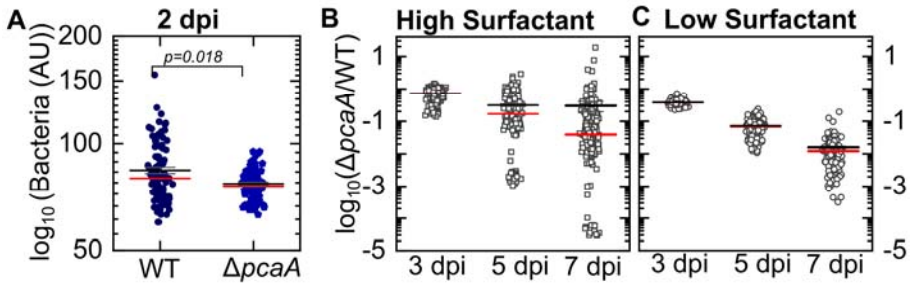

Fig. 4. LoC model in HS conditions accurately reflects *in vivo* attenuation of Δ*pcaA* mutant. Independent low-dose aerosol infections of 50 WT and Δ*pcaA* bacteria are simulated, each bacterium grows with kinetics randomly chosen from the kernel density estimations for the respective populations in Fig. 3C and 3K respectively. **(A)** In HS conditions, mean bacterial numbers for WT are significantly higher (p=0.018, n=100) than Δ*pcaA*. **(B, C)** Plots of the relative numbers of Δ*pcaA* vs WT bacteria at the indicated timepoints for HS **(B)** and LS **(C)** conditions. Each datapoint represents the mean ratio of Δ*pcaA* vs WT bacterial numbers from groups of 5 mice bootstrapped from the larger population (n=1000) for each strain. The median value of this distribution is most comparable to data from animal experiments. The attenuation is more pronounced as growth is simulated over a longer period. In all scatter plots, mean (black) and median (red) values are indicated.

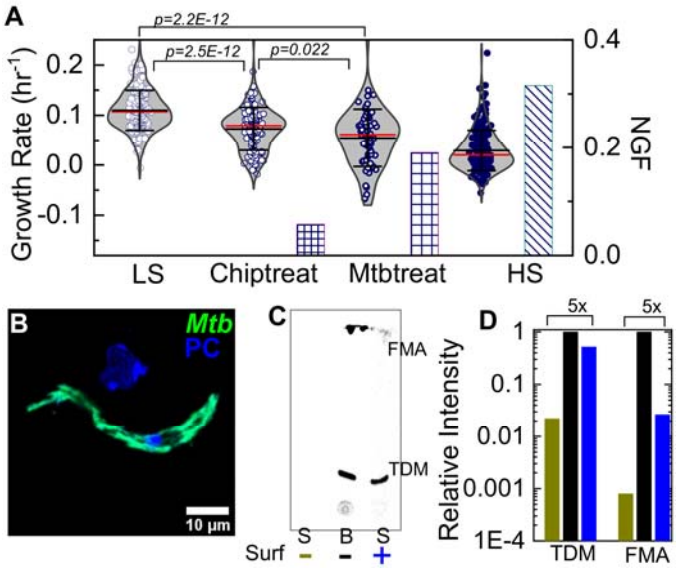

Fig. 5. Hydrophobic components of surfactant modulate host-*Mtb* first contact. (A) Scatter plots of growth rates for Mtb growth in macrophages where a LS LoC is treated with 1% Curosurf (Chiptreat), Mtb are preincubated with 1% Curosurf (Mtbtreat). Data for LS and HS conditions is included for comparison. Growth attenuation for both treatments is significant relative to LS, the non-growing fraction for the Mtbtreat condition is a significant fraction (>50%) of that in HS conditions (n=122 for LS, n=121 for Chiptreat, n=63 for Mtbtreat, and n=122 for LS). **(B)** Snapshots of fluorescent Mtb clumps post-incubation with a 1% Curosurf solution doped with 10% v/v TopFluor-Phosphatidylcholine (PC) that is false-colored blue. PC is incorporated into surfactant micelles and also coats the bacteria. **(C)** Thin Layer Chromatography for total free lipid extracts from supernatant (S) and Mtb bacteria (B) with (+) and without (-) Curosurf pre-treatment for WT. Running solvent is 90:10:1 chloroform: methanol: water, the bands are identified as sulfoglycolipids (SGL) and trehalose dimycolate (TDM). **(D)** Intensities of the SGL and TDM bands for the three samples in **(C)** are plotted

relative to that for the bacterial sample without surfactant treatment. Pulmonary surfactant removes a significant fraction of surface mycolic acids.

Materials and Methods

Cell culture

Primary C57BL/6 alveolar epithelial cells (AECs) and lung microvascular endothelial cells ('endothelial') were obtained from a commercial supplier (Cell Biologics. USA). Each vial of AECs consisted of a mix of Type I and Type II AECs, which was verified both by immunostaining (Fig. S1A-C, Fig, S1F). Both cell types were cultured in vitro in the recommended medium (complete medium) supplied by Cell Biologics in 5% CO_2 at 37°C that consisted of a base medium and supplements. In the case of lung-on-chip (LoCs) reconstituted in high surfactant (HS) conditions, AECs were seeded directly on-chip (see below), without prior *in vitro* culture. Low surfactant (LS) AECs are typically passaged 6-11 times before use.

Bone marrow isolation and culture

Bone marrow was obtained from 6-8-week-old Tg(act-EGFP) Y01Osb mice (Jackson Laboratories, USA, Stock Number 006567) and cryopreserved. This transgenic line constitutively express enhanced GFP under the control of the chicken beta-actin promoter and the cytomegalovirus enhancer. were housed in a specific pathogen-free facility. Animal protocols were reviewed and approved by EPFL's Chief Veterinarian, by the Service de la Consommation et des Affaires Vétérinaires of the Canton of Vaud, and by the Swiss Office Vétérinaire Fédéral. Bone marrow was cultured in Dulbecco's Modified Eagle Medium (DMEM) (Gibco) supplemented with 10% fetal bovine serum (FBS, Gibco) and differentiated for 7 days with 20ng/ml recombinant murine Macrophage-Colony Stimulating Factor protein (M-CSF) (Thermo Fisher Scientific). Bone marrow was cultured in plastic petri dishes without pre-sterilisation (Greiner Bio-one) so that differentiated macrophages can be subsequently detached. No antibiotics are used in the cell culture media for all cell types.

qRT-PCR

Freshly isolated AECs (HS) were grown overnight in cell-culture microdishes (Ibidi) or T-25 cell culture flask. Passaged AECs (LS) were grown to confluency in a T-25 cell culture flask. Growth media was removed from the flask, and the cells were incubated with the appropriate

volume of TRIzol (Ambion) as per the manufacturer's instruction. TRIzol treated cell lysates were stored at -20°C until further processed. At that stage RNA was precipitated with isopropanol, washed in 75% ethanol, and resuspended in 50 µl of DEPC-treated water. RNA samples were treated with Turbo DNase (Ambion) and stored at -80°C until use. DNase-treated RNA was used to generate cDNA using the SuperScript®II First-Strand Synthesis System with random hexamers (Invitrogen), which was stored at -20°C. Specific primers for *gadph*, *sftpc*, *abca3*, and *aqp5* are listed in Table S3. qRT-PCR reactions were prepared with SYBR®Green PCR Master Mix (Applied Biosystems) with 1 µM primers, and 2 µl cDNA. Reactions were run as absolute quantification on ABI PRISM®7900HT Sequence Detection System (Applied Biosystems). Amplicon specificity was confirmed by melting-curve analysis.

AEC characterization via immunofluorescence

Freshly isolated AECs (HS) or passaged AECs (LS) were grown overnight in cell-culture microdishes (Ibidi). The confluent layer of cells was subsequently fixed with 2% paraformaldehyde (Thermo Fisher Scientific) in phosphate-buffered saline (PBS, Gibco) at RT for 30 minutes, washed with PBS, and incubated with a blocking solution of 2% bovine serum albumin (BSA) in PBS for 1 hour at RT. The blocking solution was then removed, and the cells incubated with the primary antibody (1:100 dilution in 2% BSA solution in PBS) overnight at 4°C. Antibodies used were antio Podoplanin Monoclonal Antibody (eBio8.1.1 (8.1.1)), Alexa Fluor 488, eBioscience™ (ThermoFisher Scientific) and anti pro-SPC antibody (ab40879, abcam) overnight at 4C. The subsequent day, the microdishes were washed 3x in PBS and then incubated with a fluorescent secondary antibody in a solution of 2% BSA in PBS for 1 hour at RT. The microdishes were then thoroughly washed with PBS and incubated with Hoechst 33342 nuclear staining dye (1:1000 dilution, Thermo Fisher Scientific) for 15-20 minutes for nuclear staining. Confocal images were obtained on a Leica SP8 inverted microscope.

Bacterial culture

All bacterial strains were derived from *Mycobacterium tuberculosis* Erdman and cultured at 37°C. Liquid medium is Middlebrook 7H9 (Difco) supplemented with 0.5% albumin, 0.2%

glucose, 0.085% NaCl, 0.5% glycerol, and 0.02% Tyloxapol. Solid medium is Middlebrook 7H11 (Difco) supplemented with 10% OADC enrichment (Becton Dickinson) and 0.5% glycerol. Aliquots were stored in 15% glycerol at -80°C and used once to avoid loss of virulence. All strains were modified to allow constitutive expression of the fluorescent protein tdTomato under the control of the native promoter at the *attB* site. WT refers to the Erdman strain expressing tdTomato. The 5'Tn::pe35 strains was generated using transposon mutagenesis (*22*) and the ΔpcaA strain is a kind gift from the lab of Prof Michael Glickman(*26*, *27*).

Murine LoC model

Lung-chips made of polydimethylsiloxane (PDMS) were obtained from Emulate (Boston, MA). ECM coating was performed as per manufacturer instructions. Chips were activated using ER-1 solution (Emulate) dissolved in ER-2 solution at 0.5 mg/ml (Emulate) and exposed for 20 minutes under UV light. The chip was then rinsed with coating solution and exposed again to UV light for a further 20 minutes. Chips were then washed thoroughly with PBS before incubating with an ECM solution of 150 µg/ml bovine collagen type I (Atelo) and 30 µg/ml fibronectin from human plasma (Sigma-Aldrich) in PBS buffered with 15 mM HEPES solution (Gibco) for 1-2 hours at 37°C. If not used directly, coated chips were stored at 4C, and pre-activated before use by incubation for 30 minutes with the same ECM solution at 37C. Endothelial cells cultured overnight at 37°C, 5% CO_2 in T-75 cell culture flasks, detached with 0.05% Trypsin and concentrated to 5-10 million cells/ml were seeded on the bottom face of the PDMS membrane. The chip is then incubated for a short period at 37°C to allow the endothelial cells to spread and is subsequently seeded with AECs. Freshly isolated AECs are seeded directly from cryopreserved vials received from the supplier. LS LoCs are seeded from cells cultured overnight at 37°C, 5% CO_2, in both cases at a concentration of 1-2 million cells/ml. The chip is incubated overnight with complete epithelial and endothelial media in the epithelial and endothelial channel respectively under static conditions. The next day, the chip is washed and a reduced medium for the air-liquid interface (ALI) is flowed through the vascular channel using syringe pumps (Aladdin-220, Word Precision Instruments) at 60 µl/hour in a manner described

in (*43*). The components of ALI media are also described in (*43*), however we used an increased FBS concentration of 5%.

The epithelial face was incubated with epithelial base medium with 200 nM dexamethasone (Sigma Aldrich) without FBS supplementation. Flow was maintained over the subsequent 2-3 days, and the media on the epithelial face (with dexamethasone supplementation) is replaced daily. At the end of this period, GFP-expressing macrophages differentiated for 7 days in M-CSF (described above) are detached from the petri dish using a 2mM Ethylenediaminetetraacetic acid (EDTA, Sigma Aldrich) in PBS at 4C, centrifuged at 300g for 5 minutes and resuspended in a small volume of epithelial cell media without dexamethasone. This solution containing macrophages is introduced onto the epithelial face, incubated for 30 minutes at 37°C, 5% CO_2 to allow macrophages to attach to the epithelial cells. Media on the epithelial face is subsequently removed and the chip maintained overnight at ALI. Chips that successfully maintain the ALI overnight are transferred to the BSL-3 facility for Mtb infection. No antibiotics are used in all the cell culture media for setting up the LoC model.

Immunostaining of uninfected LoCs

Uninfected LoCs are maintained at an ALI for up to 7 days post-addition of the macrophages, during which time ALI media is flowed through the endothelial channel at 60 µl/hour. After 7 days at the ALI, the chip is fixed for immunostaining as described above; a permeabilization step with a 2% w/v saponin (Sigma Aldrich) and 0.1% Triton X-100 (Sigma Aldrich) solution is performed before incubation with the secondary antibody. F-actin on both the epithelial and endothelial face was stained using Sir-Actin dye (Spherochrome) at a 1µM concentration for 30 minutes concurrently with Hoechst staining as described above.

Infection of the LoC with Mtb

The chip is assembled into a stage top incubator (Okolab) prior to infection, flow is maintained using syringe pumps. 1ml of Mtb culture grown to exponential phase (optical density (OD)=0.3-0.5) is centrifuged at 5000g for 5 mins at RT, the supernatant removed, and the cells resuspended in 200 µl of epithelial cell media without FBS. A single-cell suspension is

subsequently generated via filtration through a 5µm syringe filter (Millipore). The single-cell suspension is diluted 100-fold in epithelial media, and 30 µl of this diluted single-cell suspension is added to the epithelial channel of the LoC that has so far been at ALI The infectious dose is recorded by plating further dilutions of this solution and recording colony forming units (cfu) on 7H11 plates 3-4 weeks after infection (Table S1). The chip is incubated for 2-3 hours at 37°C, 5% CO_2 to allow Mtb infection of cells on the epithelial face. At the end of this period, the solution on the epithelial face is withdrawn (in some cases, a portion of this is retained and plated for cfu to estimate the proportion of bacteria than remain on the chip (labelled 'postinf' in Table S1). The epithelial face is returned to ALI, and the inlets of the infected chip are sealed with solid pins as a safety precaution for microscopy imaging in the BSL-3 facility.

Time-lapse microscopy of the Mtb infected LoC

The LoC in the stage top incubator is placed on the stage of a widefield Nikon Ti-2 microscope, and the stage top incubator is connected to a gas mixer (Okolab) to ensure 5% CO_2 throughout the imaging period. Flow of media through the vascular channel is maintained throughout this period through the use of a syringe pump. The chip is imaged using a long working distance 20x phase contrast objective (NA=0.75, Ph2 Nikon) at either 1.5 hour or 2-hour imaging intervals. The epithelial face of the chip (where the refractive index differences are highest) is maintained in focus using the Nikon Perfect Focus System over this period. At each timepoint, a Z-stack of 9-10 images, with an axial spacing of 10 µm is taken series for a series of fields of view along the length of the chip. This is to account for the dynamic 3D movement of macrophages between both faces, as well as drift in focus over time. Each field of view is ~660 x 600 μm^2. Using a Sola SE II light source (Lumencor), macrophages and Mtb are identified through fluorescence emission in the green and red channels using GFPHQ and mcherryHQ 32 mm dichroic filters respectively. Phase contrast images are also captured, the poor quality of these images due to the refractive index differences at the ALI serves as a continuous verification that ALI is maintained. All images are captured with an Andor iXON Ultra 888 EMCCD camera cooled to -65C, with an EM gain setting of 300. This allows the sample to be illuminated with a low intensity of incident light in all fluorescent channels, and reduced photodamage. Co-

localization of these signals over a time course is identified as consistent with macrophage infection. On the other hand, Mtb bacteria that do not co-localize with a macrophage are assumed to infect AECs, which can be verified by subsequent immunostaining.

Data analysis

Data is first visualized using ImageJ where macrophage and AEC infection from each field of view is visually curated, considering the co-localization of fluorescent signals over time. Smaller stacks of 1-2 microcolonies are assembled. Custom-written software in MATLAB is used to measure the total fluorescence intensity of each microcolony and uses the nestedSortStruct algorithm for MATLAB written by the Hughey lab (Jake Hughey (2020). nestedSortStruct (https://www.github.com/hugheylab/nestedSortStruct), GitHub). Briefly, at each timepoint, the Z-stack with the highest intensity in the fluorescence channel was identified, this image is then segmented to identify the microcolony, and total fluorescence measured by summing the intensity of all the pixels in this region, after subtracting a value for each pixel that represented the average background fluorescence in this channel. We choose the total fluorescence intensity because it accounts for both bacterial growth and dilution of the fluorescent protein (which is low in a slow-growing bacterium like Mtb). We are unable to measure the volume of the microcolony accurately due to the choose to very poor axial resolution using widefield imaging with refractive index differences at ALI, therefore we obtain this value from only the Z stack with the highest intensity. Statistical analysis is performed using Origin 9.2 (OriginLabs). P-values are calculated using a Kruskal-Wallis one-way ANOVA test, with the null hypothesis that the medians of each population are equal.

Simulations of in vivo infections

Growth rate datasets for WT, 5'Tn::*pe35*, and Δ*pcaA* strains in HS and LS conditions were fitted with a non-parametric Kernel Smoothed distribution. We simulated a low-dose aerosol infection of 50 bacteria in the alveolar space of n=100 or n=100 mice, and conservatively assumed that every bacterium interacted with a macrophage upon first contact, as we do not have a reliable estimate for the frequency of AEC infection *in vivo* (although it is likely to be low).

Each bacterium was assigned a growth rate picked at random from the Kernel Smoothed distributions and assumed to grow exponentially with these growth rates to generate a microcolony. The total bacterial numbers in each mouse at 2, 3, 5, and 7 days post infection were obtained by summing the bacterial counts from each microcolony for each mouse. Total bacterial numbers for n=100 mice of WT and ΔpcaA 5'Tn::*pe35* are shown in Fig. 4A and Fig. S6A respectively. To compare relative attenuation of the ΔpcaA strains.

Curosurf treatment of LS LoCs

Curosurf (Chiesi Pharmaceuticals) was purchased and used as a 1% solution in epithelial media for all experiments. In the case where Curosurf was added to a LS LoC, a 1% solution was introduced to the epithelial face after the macrophages were added but before ALI was introduced for 2 minutes, and then removed. The following morning, this procedure was repeated just prior to the addition of the single-cell suspension of Mtb in the manner described above. Alternatively, 1ml of Mtb in exponential phase in 7H9 media was centrifuged at 5000g for 5 minutes and resuspended in 1ml of 1% cell culture media and incubated for 10-15 mins at room temperature. This solution was then centrifuged again at 5000g for 5 minutes and a single-cell Mtb suspension was generated as described above. Fluorescent labelling of surfactant was achieved by adding TopFluor phosphatidylcholine (10% v/v, Avanti Polar Lipids) to Curosurf before dilution in cell culture media.

Total free lipid extraction and thin-liquid chromotgraphy (TLC)

10ml Mtb cultures were grown till stationary phase in 7H9 with 10 μC_i of ^{14}C propionate added during exponential phase. Total free lipid extraction from bacterial pellet, supernatant, and the supernatant from bacteria pre-treated with a 3% Curosurf solution for 15 mins at 37C were extracted as described (*44*). Extracted free lipids were air-dried, resuspended in 2:1 v/v solution of cholorform:methanol and aliquots were spotted on 5 x 10 cm TLC silica gel 60 F_{254} (Merck). Running solvent was 90:10:1 chloroform:ethanol:water and the developed TLC plate was exposed to an Amersham Hyperfilm ECl (GE Healthcare) for phosphorescence imaging and

visualised with a Typhoon scanner (GE Healthsciences). Intensities of the bands observed was quantified using ImageJ.

Bibliography

1. http://www.who.int/tdr/publications/tdr-research-publications/incentives-disincentives-anti-tuberculosis/en/.

2. B. Ma, C. Darquenne, Aerosol deposition characteristics in distal acinar airways under cyclic breathing conditions. *J. Appl. Physiol.* **110**, 1271–1282 (2011).

3. G. Fedorovitch, in *Rhinosinusitis [Working Title]* (IntechOpen, 2019).

4. E. R. Weibel, On the Tricks Alveolar Epithelial Cells Play to Make a Good Lung. *Am. J. Respir. Crit. Care Med.* **191**, 504–513 (2015).

5. L. Huang, E. V. Nazarova, S. Tan, Y. Liu, D. G. Russell, Growth of Mycobacterium tuberculosis in vivo segregates with host macrophage metabolism and ontogeny. *J. Exp. Med.* **215** (2018) (available at http://jem.rupress.org/content/215/4/1135?utm_source=TrendMD&utm_medium=cpc&utm_campaign=JEM_TrendMD-1).

6. A. V. Misharin, L. Morales-Nebreda, P. A. Reyfman, C. M. Cuda, J. M. Walter, A. C. McQuattie-Pimentel, C. I. Chen, K. R. Anekalla, N. Joshi, K. J. N. Williams, H. Abdala-Valencia, T. J. Yacoub, M. Chi, S. Chiu, F. J. Gonzalez-Gonzalez, K. Gates, A. P. Lam, T. T. Nicholson, P. J. Homan, S. Soberanes, S. Dominguez, V. K. Morgan, R. Saber, A. Shaffer, M. Hinchcliff, S. A. Marshall, A. Bharat, S. Berdnikovs, S. M. Bhorade, E. T. Bartom, R. I. Morimoto, W. E. Balch, J. I. Sznajder, N. S. Chandel, G. M. Mutlu, M. Jain, C. J. Gottardi, B. D. Singer, K. M. Ridge, N. Bagheri, A. Shilatifard, G. R. S. Budinger, H. Perlman, Monocyte-derived alveolar macrophages drive lung fibrosis and persist in the lung over the life span. *J. Exp. Med.* **214**, 2387–2404 (2017).

7. J. M. Scordo, D. L. Knoell, J. B. Torrelles, Alveolar Epithelial Cells in Mycobacterium tuberculosis Infection: Active Players or Innocent Bystanders? *J. Innate Immun.* **8**, 3–14 (2016).

8. J. S. Ferguson, D. R. Voelker, F. X. McCormack, L. S. Schlesinger, Surfactant protein D binds to Mycobacterium tuberculosis bacilli and lipoarabinomannan via carbohydrate-lectin interactions resulting in reduced phagocytosis of the bacteria by macrophages. *J. Immunol.* **163**, 312–21 (1999).

9. J. M. Scordo, J. Arcos, H. V. Kelley, L. Diangelo, S. J. Sasindran, E. Youngmin, M. D. Wewers, S.-H. Wang, J.-M. Balada-Llasat, J. B. Torrelles, Mycobacterium tuberculosis

Cell Wall Fragments Released upon Bacterial Contact with the Human Lung Mucosa Alter the Neutrophil Response to Infection. *Front. Immunol.* **8**, 307 (2017).

10. J. Arcos, S. J. Sasindran, N. Fujiwara, J. Turner, L. S. Schlesinger, J. B. Torrelles, Human Lung Hydrolases Delineate Mycobacterium tuberculosis –Macrophage Interactions and the Capacity To Control Infection . *J. Immunol.* **187**, 372–381 (2011).

11. F. M. Collins, I. M. Orme, in *Tuberculosis* (American Society of Microbiology, 1994; http://www.asmscience.org/content/book/10.1128/9781555818357.chap8), pp. 113–134.

12. K. Westphalen, G. A. Gusarova, M. N. Islam, M. Subramanian, T. S. Cohen, A. S. Prince, J. Bhattacharya, Sessile alveolar macrophages communicate with alveolar epithelium to modulate immunity. *Nature*. **506**, 503–506 (2014).

13. M. R. Looney, E. E. Thornton, D. Sen, W. J. Lamm, R. W. Glenny, M. F. Krummel, Stabilized imaging of immune surveillance in the mouse lung. *Nat. Methods*. **8**, 91–96 (2011).

14. T. R. Lerner, S. Borel, D. J. Greenwood, U. Repnik, M. R. G. Russell, S. Herbst, M. L. Jones, L. M. Collinson, G. Griffiths, M. G. Gutierrez, Mycobacterium tuberculosis replicates within necrotic human macrophages. *J. Cell Biol.* (2017).

15. D. Huh, B. D. Matthews, A. Mammoto, M. Montoya-Zavala, H. Y. Hsin, D. E. Ingber, Reconstituting organ-level lung functions on a chip. *Science*. **328**, 1662–8 (2010).

16. B. Grigoryan, S. J. Paulsen, D. C. Corbett, D. W. Sazer, C. L. Fortin, A. J. Zaita, P. T. Greenfield, N. J. Calafat, J. P. Gounley, A. H. Ta, F. Johansson, A. Randles, J. E. Rosenkrantz, J. D. Louis-Rosenberg, P. A. Galie, K. R. Stevens, J. S. Miller, Multivascular networks and functional intravascular topologies within biocompatible hydrogels. *Science*. **364**, 458–464 (2019).

17. A. Jain, R. Barrile, A. van der Meer, A. Mammoto, T. Mammoto, K. De Ceunynck, O. Aisiku, M. Otieno, C. Louden, G. Hamilton, R. Flaumenhaft, D. Ingber, Primary Human Lung Alveolus-on-a-chip Model of Intravascular Thrombosis for Assessment of Therapeutics. *Clin. Pharmacol. Ther.* **103**, 332–340 (2018).

18. A. M. Ghaemmaghami, M. J. Hancock, H. Harrington, H. Kaji, A. Khademhosseini, Biomimetic tissues on a chip for drug discovery. *Drug Discov. Today*. **17**, 173–81 (2012).

19. K. Ronaldson-Bouchard, G. Vunjak-Novakovic, Organs-on-a-Chip: A Fast Track for Engineered Human Tissues in Drug Development. *Cell Stem Cell*. **22**, 310–324 (2018).

20. A. Grassart, V. Malardé, S. Gobba, A. Sartori-Rupp, J. Kerns, K. Karalis, B. Marteyn, P. Sansonetti, N. Sauvonnet, Bioengineered Human Organ-on-Chip Reveals Intestinal Microenvironment and Mechanical Forces Impacting Shigella Infection. *Cell Host*

Microbe. **26**, 435-444.e4 (2019).

21. J. B. Torrelles, L. S. Schlesinger, Integrating Lung Physiology, Immunology, and Tuberculosis. *Trends Microbiol.* **25**, 688–697 (2017).

22. J. M. Chen, M. Zhang, J. Rybniker, S. Boy-Röttger, N. Dhar, F. Pojer, S. T. Cole, *Mycobacterium tuberculosis* EspB binds phospholipids and mediates EsxA-independent virulence. *Mol. Microbiol.* **89**, 1154–1166 (2013).

23. N. van der Wel, D. Hava, D. Houben, D. Fluitsma, M. van Zon, J. Pierson, M. Brenner, P. J. Peters, M. tuberculosis and M. leprae Translocate from the Phagolysosome to the Cytosol in Myeloid Cells. *Cell*. **129**, 1287–1298 (2007).

24. M. B. Ryndak, K. K. Singh, Z. Peng, S. Laal, Transcriptional Profile of Mycobacterium tuberculosis Replicating in Type II Alveolar Epithelial Cells. *PLoS One*. **10**, e0123745 (2015).

25. J. Raffetseder, N. Iakobachvili, V. Loitto, P. J. Peters, M. Lerm, Retention of EsxA in the Capsule-Like Layer of *Mycobacterium tuberculosis* Is Associated with Cytotoxicity and Is Counteracted by Lung Surfactant. *Infect. Immun.* **87** (2019), doi:10.1128/IAI.00803-18.

26. M. S. Glickman, J. S. Cox, W. R. Jacobs, A Novel Mycolic Acid Cyclopropane Synthetase Is Required for Cording, Persistence, and Virulence of Mycobacterium tuberculosis. *Mol. Cell*. **5**, 717–727 (2000).

27. V. Rao, N. Fujiwara, S. A. Porcelli, M. S. Glickman, Mycobacterium tuberculosis controls host innate immune activation through cyclopropane modification of a glycolipid effector molecule. *J. Exp. Med.* **201**, 535–43 (2005).

28. E. J. Peterson, R. Bailo, A. C. Rothchild, M. L. Arrieta□Ortiz, A. Kaur, M. Pan, D. Mai, A. A. Abidi, C. Cooper, A. Aderem, A. Bhatt, N. S. Baliga, Path□seq identifies an essential mycolate remodeling program for mycobacterial host adaptation. *Mol. Syst. Biol.* **15** (2019), doi:10.15252/msb.20188584.

29. D. Pisu, L. Huang, J. K. Grenier, D. G. Russell, Dual RNA-Seq of Mtb-Infected Macrophages In Vivo Reveals Ontologically Distinct Host-Pathogen Interactions. *Cell Rep.* **30**, 335-350.e4 (2020).

30. E. J. Muñoz-Elías, J. D. McKinney, Mycobacterium tuberculosis isocitrate lyases 1 and 2 are jointly required for in vivo growth and virulence. *Nat. Med.* **11**, 638–44 (2005).

31. T. N. Finley, A. J. Ladman, Low Yield of Pulmonary Surfactant in Cigarette Smokers. *N. Engl. J. Med.* **286**, 223–227 (1972).

32. S. Subramaniam, Biochemical and Biophysical Characterization of Pulmonary Surfactant

in Rats Exposed Chronically to Cigarette Smoke. *Fundam. Appl. Toxicol.* **27**, 63–69 (1995).

33. J. I. Moliva, M. A. Duncan, A. Olmo-Fontánez, A. Akhter, E. Arnett, J. M. Scordo, R. Ault, S. J. Sasindran, A. K. Azad, M. J. Montoya, N. Reinhold-Larsson, M. V. S. Rajaram, R. E. Merrit, W. P. Lafuse, L. Zhang, S.-H. Wang, G. Beamer, Y. Wang, K. Proud, D. J. Maselli, J. Peters, S. T. Weintraub, J. Turner, L. S. Schlesinger, J. B. Torrelles, The Lung Mucosa Environment in the Elderly Increases Host Susceptibility to Mycobacterium tuberculosis Infection. *J. Infect. Dis.* **220**, 514–523 (2019).

34. M. Gonzalez-Juarrero, J. M. Hattle, A. Izzo, A. P. Junqueira-Kipnis, T. S. Shim, B. C. Trapnell, A. M. Cooper, I. M. Orme, Disruption of granulocyte macrophage-colony stimulating factor production in the lungs severely affects the ability of mice to control *Mycobacterium tuberculosis* infection. *J. Leukoc. Biol.* **77**, 914–922 (2005).

35. L. E. Bermudez, F. J. Sangari, P. Kolonoski, M. Petrofsky, J. Goodman, The efficiency of the translocation of Mycobacterium tuberculosis across a bilayer of epithelial and endothelial cells as a model of the alveolar wall is a consequence of transport within mononuclear phagocytes and invasion of alveolar epithelial cells. *Infect. Immun.* **70**, 140–6 (2002).

36. D. Ganbat, S. Seehase, E. Richter, E. Vollmer, N. Reiling, K. Fellenberg, K. I. Gaede, C. Kugler, T. Goldmann, Mycobacteria infect different cell types in the human lung and cause species dependent cellular changes in infected cells. *BMC Pulm. Med.* **16**, 19 (2016).

37. M. K. Bielecka, L. B. Tezera, R. Zmijan, F. Drobniewski, X. Zhang, S. Jayasinghe, P. Elkington, A Bioengineered Three-Dimensional Cell Culture Platform Integrated with Microfluidics To Address Antimicrobial Resistance in Tuberculosis. *MBio*. **8**, e02073-16 (2017).

38. V. R. Parasa, M. J. Rahman, A. T. N. Hoang, M. Svensson, S. Brighenti, M. Lerm, Modeling Mycobacterium tuberculosis early granuloma formation in experimental human lung tissue. *DMM Dis. Model. Mech.* **7**, 281–288 (2014).

39. J. S. Ferguson, D. R. Voelker, J. A. Ufnar, A. J. Dawson, L. S. Schlesinger, Surfactant Protein D Inhibition of Human Macrophage Uptake of Mycobacterium tuberculosis Is Independent of Bacterial Agglutination . *J. Immunol.* **168**, 1309–1314 (2002).

40. J. S. Ferguson, J. L. Martin, A. K. Azad, T. R. McCarthy, P. B. Kang, D. R. Voelker, E. C. Crouch, L. S. Schlesinger, Surfactant protein D increases fusion of Mycobacterium tuberculosis- containing phagosomes with lysosomes in human macrophages. *Infect. Immun.* **74**, 7005–7009 (2006).

41. R. Pasula, J. F. Downing, J. R. Wright, D. L. Kachel, T. E. Davis, W. J. Martin, Surfactant

Protein A (SP-A) Mediates Attachment of *Mycobacterium tuberculosis* to Murine Alveolar Macrophages. *Am. J. Respir. Cell Mol. Biol.* **17**, 209–217 (1997).

42. T. Kimoto, D. Mizuno, T. Takei, T. Kunimi, S. Ono, S. Sakai, H. Kido, Intranasal influenza vaccination using a new synthetic mucosal adjuvant SF-10: Induction of potent local and systemic immunity with balanced Th1 and Th2 responses. *Influenza Other Respi. Viruses*. **7**, 1218–1226 (2013).

43. B. A. Hassell, G. Goyal, E. Lee, A. Sontheimer-Phelps, O. Levy, C. S. Chen, D. E. Ingber, Human Organ Chip Models Recapitulate Orthotopic Lung Cancer Growth, Therapeutic Responses, and Tumor Dormancy In Vitro. *Cell Rep.* **21**, 508–516 (2017).

44. T. Parish, D. M. Roberts, *Mycobacteria protocols: Third edition* (Springer New York, 2015).